Organic Electronics 45 (2017) 97–103

Contents lists available at ScienceDirect

Organic Electronics

journal homepage: www.elsevier.com/locate/orgel

Enhanced performance of inverted perovskite solar cells using solution-processed carboxylic potassium salt as cathode buffer layer

Zhao Hu [a], Jingsheng Miao [a], Ming Liu [a], Tingbin Yang [b, **], Yongye Liang [b], Osamu Goto [a], Hong Meng [a, *]

[a] School of Advanced Materials, Peking University Shenzhen Graduate School, Shenzhen 518055, China
[b] Department of Materials Science and Engineering, South University of Science and Technology of China, Shenzhen 518055, China

ARTICLE INFO

Article history:
Received 13 December 2016
Received in revised form
13 February 2017
Accepted 26 February 2017
Available online 28 February 2017

Keywords:
Perovskite solar cell
Interfacial engineering
Cathode buffer layer
Carboxylic potassium salt

ABSTRACT

Using a novel solution-processed carboxylic potassium salt (F-R-COOK) as cathode buffer layer (CBL), a power conversion efficiency (PCE) of 14.37% is obtained, which is more than 51% increase compared with that of the Ag-only device under similar fabrication conditions. The test result of single electron devices and Electrochemical impedance spectroscopy (EIS) measurements demonstrate that the interlayer decreases charge transport resistance. Ultraviolet photoelectron spectroscopy (UPS) measurements are used to study the interfacial effects induced by the new CBL. It is found that F-R-COOK can reduce the work function of the Ag electrode by forming desired interfacial dipoles. Our work indicates the promising applications of F-R-COOK based CBL in perovskite solar cells and may provide some insights into the design and synthesis of new interfacial materials to further improve the device performance.

1. Introduction

Interfacial engineering is a key technique for the enhanced performance of organic electronic devices, including organic light emitting diodes (OLED) [1], organic thin film transistors (OTFT) [2], and organic photovoltaic (OPVs) [3]. Perovskite solar cells (PVSCs) based on hybrid methylammonium lead halide ($CH_3NH_3PbX_3$, X = halogen) have been widely researched [4–13] and considered to be one of the most promising next generation energy conversion technologies. Perovskite materials offer a broad range of attractive features such as low-cost of precursors, broad optical absorbance, long exciton diffusion length, solution processability and high mechanical flexibility [14–17].The power conversion efficiency (PCE) over 20% has been reported and a record PCE of 22.1% has been certified [18]. However, the fabrication of most efficient perovskite solar cells is typically developed by employing a high-quality condensed TiO_2 layer as electron transporting layer, which requires high-temperature processing (450 °C) for a long time [19,20]. While, high performance perovskite solar cells can also be fabricated using a hybrid planar heterojunction (PHJ), in which the common device architecture is sandwiched between a hole-transport layer, and an electron-transport layer [6,6],-phenyl-C_{61}-butyric acid methyl (PCBM). This structure is considered to have the most promising commercialization due to its relatively simple device architecture and potential for being fabricated at low-temperature, using large-area coating processes [17,21–24]. Nevertheless, the barrier at the contact interface between the Fermi level of various electrode metals (e.g., Ag, Au) and the lowest unoccupied molecular orbital (LUMO) of the organic material (PCBM) still exists in organic optoelectronic devices, leading to poor electron injection and extraction [25,26]. The charge injection and extraction at the metal-organic material interface has a significant influence on the electrical properties of the optoelectronic devices. Therefor, to reduce the contact barrier, the interface between the metal electrode and the PCBM layer should be optimized. The success of applying the interfacial materials to enhance the performance in organic solar cells directs the interface design rules for perovskite solar cell technology. This method has led to put more efforts in interfacial engineering of PVSCs. High fill factors were achieved with e.g., the use of thermal vapor deposited LiF [27], bathocuproine (BCP) [23,28], or fullerene (C60) [22]on top of the PCBM layer. All these strategies improved the contact properties and improved the device efficiency. While, the processing of these materials requires high temperature and vacuum, which increases the processing time and production cost. It is worth to mention that Zhang et al. developed highly efficient inverted PVSCs by inserting an ultrathin PEIE layer as the CBL [29]. In addition, the Bis-C_{60} surfactant [30], thiol-functionalized cation surfactant [31], n-doped metal

* Corresponding author.
** Corresponding author.
E-mail address: menghong@pkusz.edu.cn (H. Meng).

http://dx.doi.org/10.1016/j.orgel.2017.02.041
1566-1199/

oxides [32], amino-functionalized polymer (PN4N) [33] and amino-functionalized small molecules (C_{60}-N [34], PDINO [35]) were also employed as an efficient CBL to modify the interface between the PCBM and top metal contact. These works highlighted the direction of developing solution-processed cathode interlayers for inverted PVSCs, allowing one to optimize the device performance. Compared to polymers, small molecules are more attractive because of their advantages including easy synthesis without complex polymerization, easy to purify, monodisperse with a well-defined chemical structure and have batch-to-batch reproducibility. In this paper, we designed a novel oligomeric fluorene cathode interlayer with carboxylic acid potassium as the end group. With the end-group changing from carboxyl to carboxylic acid potassium, its solubility in alcohol varies from insoluble to easily soluble. Moreover, in this case, when spin-coating the interfacial layer PCBM would not be washed away. Meanwhile, the F-R-COOK backbone is an n-type unit which can achieve high adhesion to the active layer [36]. This molecule was applied as CBL in PHJ PVSCs, with the device configuration of ITO/NiO_x/Perovskite Layer/PCBM/F-R-COOK/Ag (Fig. 1a), of which NiO_x has been previously demonstrated as high efficient HTL [37]. A cross-sectional scanning electron microscopy (SEM) image of the device with the F-R-COOK CBL is shown in Fig. 1b. For comparison, the devices without CBL were also fabricated under the same conditions. By inserting the F-R-COOK layer, the device power conversion efficiency (PCE) can increase from 9.51% to 14.37%. Comparing with the control devices, the short circuit current (J_{sc}), fill factor (*FF*), open circuit voltage (V_{oc}) and PCE of the devices with F-R-COOK layer are significantly improved.

2. Material and methods

2.1. Synthesis of F-R-COOH and F-R-COOK

The representative synthesis process of F-R-COOH and F-R-COOK is shown in Scheme 1. 9, 9-dioctylfluorene-2, 7-bis (boronic acid pinacol ester), 2-Bromo-5-formylthiophene and rhodanine-3-acetic acid were obtained from commercial suppliers without further purification. And all metal catalysts were purchased from TCI.

2.1.1. Synthesis of F-CHO

A nitrogen flushed round bottom flask was charged with 9, 9-dioctylfluorene-2, 7-bis (boronic acid pinacol ester) (5.2 g, 8 mmol), 2-Bromo-5-formylthiophene (6.12 g, 32 mmol), K_2CO_3 (6.64 g, 48 mmol) and $Pd(PPh_3)_4$ (139 mg, 0.12 mmol). Toluene (72 ml) and H_2O (24 ml) were then added and the mixture was bubbled with nitrogen for 15min. The mixture was refluxed for 24 h before quenching by water. The solution was extracted with CH_2Cl_2 for three times and organic layer was dried with Na_2SO_4 for 2 h. After removal of solvent, the crude product was purified by column chromatography on silica gel (eluent: CH_2Cl_2: petroleum ether = 1:1) to afford a yellow solid (3.6 g, 72% yield). 1H NMR (*$CDCl_3$* 300 MHz) δ 9.91 (s, 2H), 7.78–7.75 (m, 4H), 7.71 (d, J = 1.5 Hz, 1H), 7.68 (d, J = 1.8 Hz, 1H), 7.64 (d, J = 1.2 Hz, 2H), 7.49 (d, J = 3.9 Hz, 2H), 2.03 (m, 4H), 1.05 (m, 20H), 0.78 (t, J = 13.8 Hz, 6H), 0.660 (m, 4H).

2.1.2. Synthesis of F-R-COOH

F-CHO (200 mg, 0.33 mmol), ammonium acetate (0.51 g, 6.6 mmol) and rhodanine-3-acetic acid (1.26 g, 6.6 mmol) were dissolved in 20 ml acetic acid glacial. The mixture was refluxed for 24 h and then poured into water. The precipitation solid was washed with methanol to afford a red solid (220 mg, 70% yield). ^{1}H NMR (DMSO-d_6 300 MHz) δ 8.16 (s, 2H), 7.90–7.85 (m, 8H), 7.78 (dd, J = 8 Hz, 1.5 Hz, 2H), 4.72 (s, 4H), 2.11 (m, 4H), 1.02 (m, 20H), 0.70 (t, J = 13.5 Hz, 6H), 0.55 (m, 4H). ^{13}C NMR (DMSO-d_6 300 MHz) δ 192.18, 167.70, 166.41, 153.24, 152.21, 141.49, 136.59, 132.17, 126.33, 121.48, 118.86, 99.90, 55.64, 31.58, 29.44, 28.84, 23.66, 22.43, 14.25. MS (MALDI-TOF) m/z: calculated for $C_{49}H_{52}N_2O_6NaS_6$, $[M+Na]^+$, 979.2047; found 979.2055.

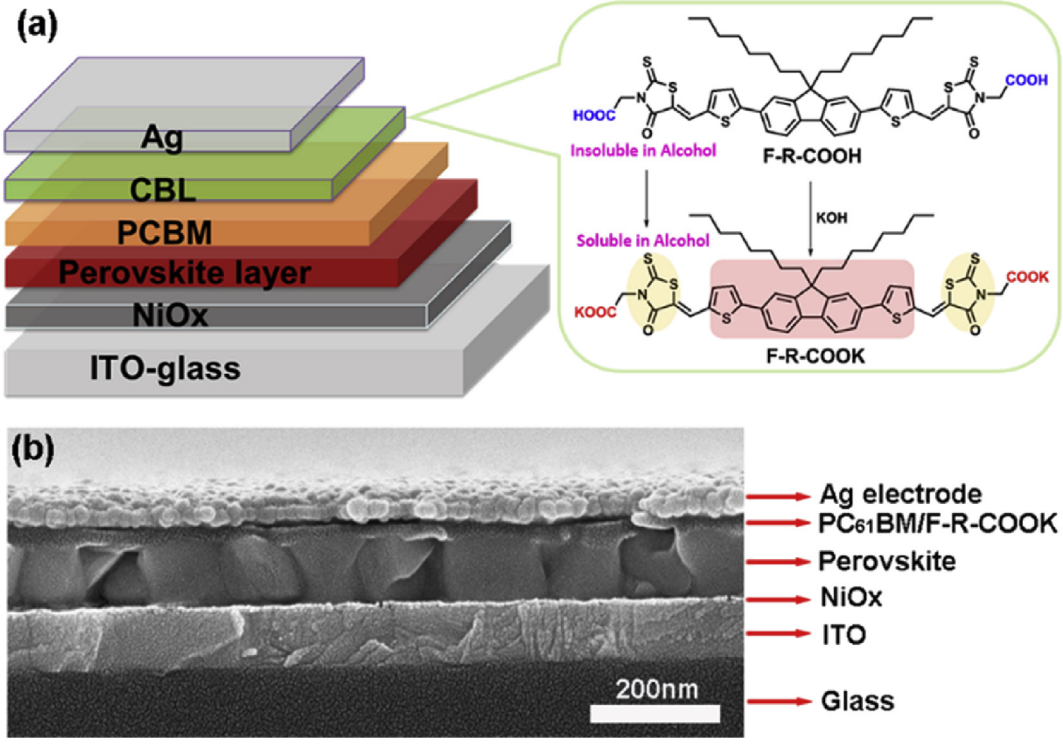

Fig. 1. a) Device architecture and the molecular structure of F-R-COOH and F-R-COOK, (b) Cross-sectional SEM image of the device.

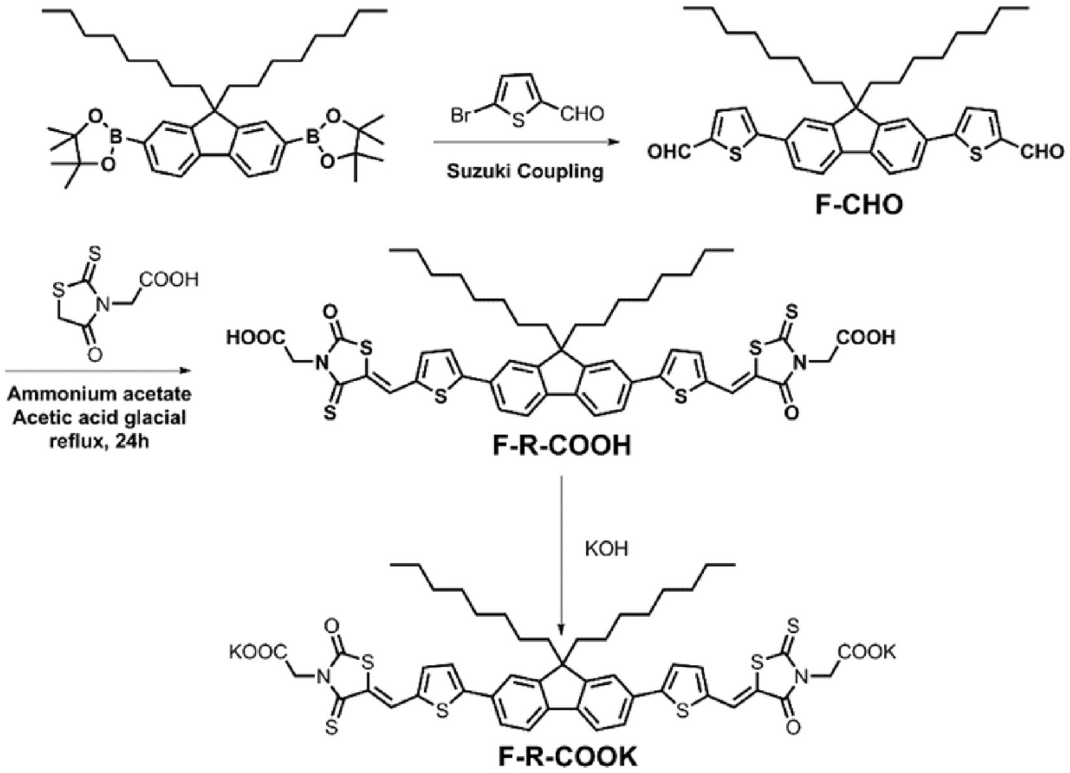

Scheme 1. Synthetic route of F-R-COOK.

2.1.3. Synthesis of F-R-COOK

F-R-COOH (100 mg, 0.1 mmol) and KOH (11.74 mg, 0.2 mmol) were dissolved in CH_2Cl_2. The mixture was stirred at room temperature for 24 h. The reaction mixture was then washed with water, and dried over Na_2SO_4. After removal of the solvent, the resulting product was dried in vacuum at 60 °C for 48 h to yield F-R-COOK (85 mg, 83% yield).

2.2. Materials characterization

Nuclear magnetic resonance (NMR) was taken on Bruker AVANCE III 300 MHz and 400 MHz Spectrometer. All chemical shifts were reported relative to tetramethylsilane (TMS) at 0.0 ppm, unless otherwise stated.

High resolution mass spectra were obtained from a MALDI-TOF Mass Spectrometer.

The absorption spectrum was recorded with UV–visible spectrophotometer (Shimadzu 2450). Cyclic voltammetry was determined by electrochemical workstation (Chenhua CHI600E).

2.3. Device fabrication

2.3.1. Materials

PC61BM was purchased from Solenne BV. Dimethyl sulfoxide DMSO and γ-butyrolactone were purchased from TCI and used as received without further purification. Lead(II) iodide(PbI_2), Lead(II) chloride ($PbCl_2$),$NiNO_3 \cdot 6H_2O$, hydroiodic acid (99.99%) and methylamine were purchased from Sigma-Aldrich and used as received without further purification. Methlammonium iodide (MAI) was synthesized in our labs according the literature [36].

2.3.2. Solar cell fabrication and testing

Indium tin oxide (ITO) is used as the substrate and was cleaned prior to device fabrication by sonication in acetone, detergent, deionized water and isopropyl alcohol sequentially, followed by baking at 80 °C in vacuum oven for 12 h. NiOx thin film were prepared according the published procedure [38]. To prepare the perovskite precursor solution, MAI with PbI_2 and $PbCl_2$ as a molar ratio of 1:0.85:0.15 were dissolved in γ-butyrolactone and DMSO with a volume ratio of 7:3 and stirred at 60 °C for 6 h. Then, the perovskite precursor solution was spin-coated onto the ITO/NiOx substrate at 1000 rpm for 20 s and 5000 rpm for 30s and washed with toluene after 20 s at 5000 rpm. The substrates were thermal annealed at 100 °C for 10 min. The electron transport layer ($PC_{61}BM$, 10 mg/ml in chloroform) was spin-coated onto the perovskite layer at 2000 rpm for 30 s followed by spun casting the F-R-COOK. The F-R-COOK was dissolved in the methanol with concentration of 2 mg/ml and filtered with 0.45 μm PTFE filter. Finally, a 90 nm Ag film was evaporated through a shadow mask in a vacuum chamber under a pressure of 1×10^{-4} pa. The active area of the device was 0.045 cm^2. The *J-V* characteristics were measured by a Keithley 2400 source-measurement unit under AM 1.5G (100 mW/cm^2) spectrum from a solar simulator (Newport, Oriel AM 1.5G, 100 mW/cm^2). The light intensity is calibrated using an NREL-certified monocrystalline Si diode coupled to a KG3 filter. The incident photon-to-current efficiency spectra were measured by a solar cell photodetector responsivity measurement system (Enlitech, Inc.)

2.3.3. PC61BM electron only device fabrication

The *J-V* characteristics of $PC_{61}BM$ electron-only device measured with device structure of ITO/ZnO (30 nm)/$PC_{61}BM$ (110 nm)/ without or with F-R-COOK/Ag (90 nm), The $PC_{61}BM$ layer films were prepared by dissolving $PC_{61}BM$ in chloroform, followed by spin-coating on top of the ZnO layer. Then, F-R-COOK in methanol with concentration of 2 mg/ml was spin-coated onto the $PC_{61}BM$ or without. Finally, The 90 nm Ag was evaporated through a shadow mask in a vacuum chamber under a pressure of 1×10^{-4} Pa.

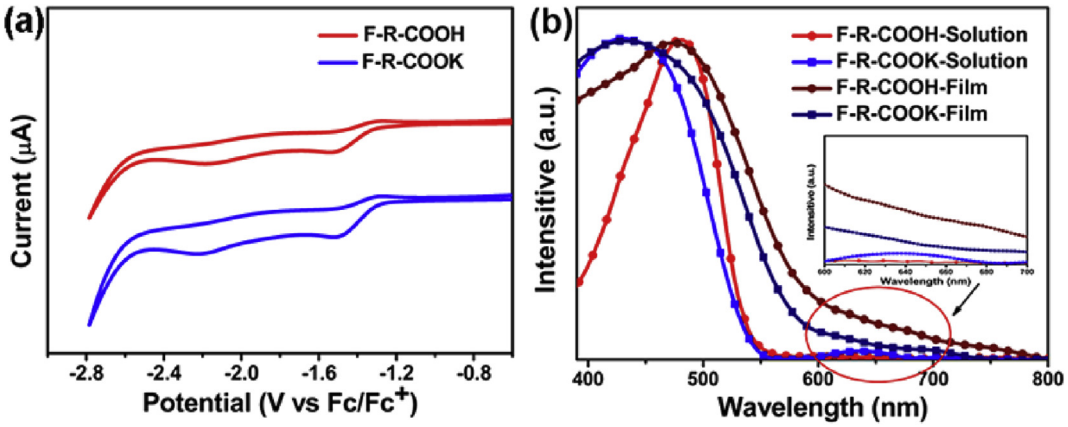

Fig. 2. a) Cyclic voltammograms of F-R-COOH and F-R-COOK. b) UV–vis spectra of F-R-COOH and F-R-COOK in solution and thin film.

3. Results and discussions

The cyclic voltammograms (CV) of F-R-COOH and F-R-COOK are shown in Fig. 2a, their LUMO energy levels are estimated, respectively, to be −3.45 eV and −3.55 eV. The corresponding UV–vis absorption spectra of F-R-COOH and F-R-COOK in 10^{-5} M, methanol and in solid film are displayed in Fig. 2b. Compared with F-R-COOH, a new comparatively weak absorption band emerging at 640 nm for F-R-COOK solution implying the evident effect of the formation of radical-cations. The optical band gaps estimated from the onset of the absorption (in solid film) is 2.0 eV for F-R-COOH and 2.1 eV for F-R-COOK. The HOMO energy levels are calculated to be −5.46 and −5.55 eV for F-R-COOH and F-R-COOK, respectively. F-R-COOH and F-R-COOK show quite similar values of the optical band gaps, HOMO and LUMO energy levels. It indicates that the potassium ion has no obvious influence on the energy levels of F-R-COOK.

To investigate the interfacial modification effect of F-R-COOK as cathode interlayer on the performance of PVSCs, we fabricated perovskite solar cells with the device structure of ITO/NiO_x/Perovskite Layer/PCBM/CBL/Ag as shown in Fig. 1a. The cathode interlayers were prepared by spin-coating the methanol solution. For comparison, the devices without CBL were also fabricated and

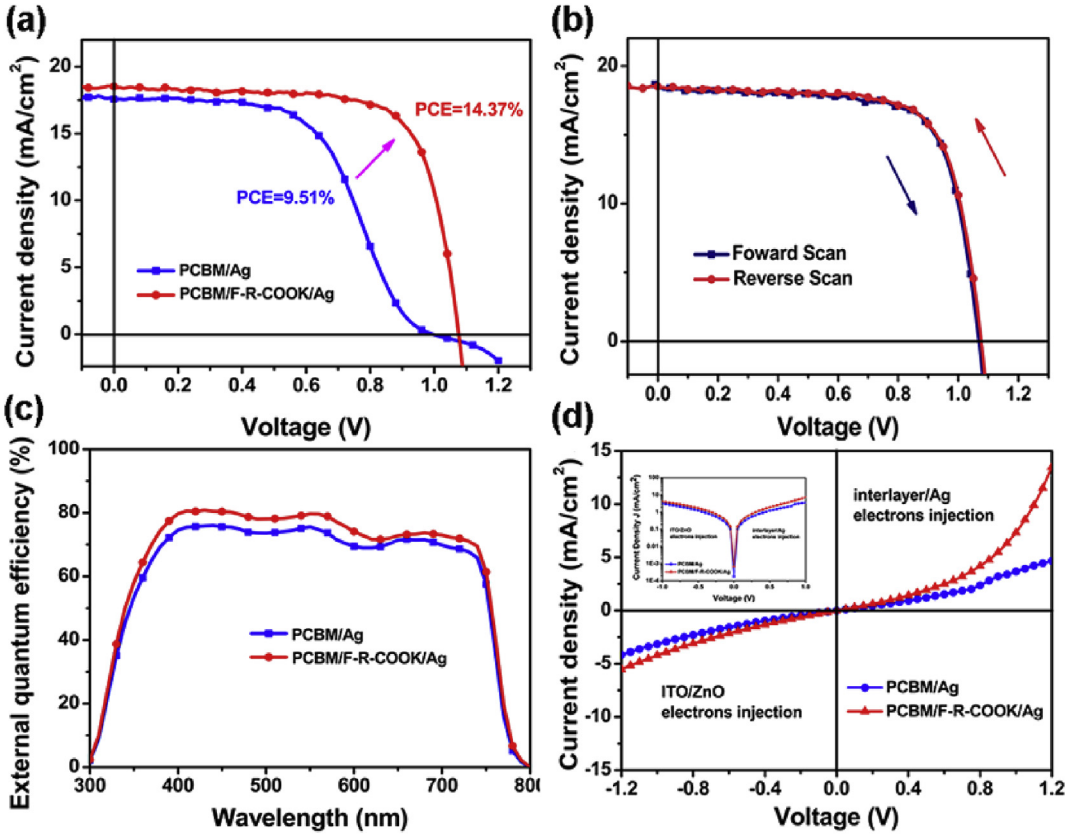

Fig. 3. a) *J-V* curve of the devices with and without a F-R-COOK modification layer, b) hysteresis investigation of the device with F-R-COOK interlayer, c) EQE spectra of the corresponding solar cells, d) Current density versus voltage characteristics of ITO/ZnO/PCBM (100 nm) with and without F-R-COOK interlayers/Ag electron-only devices. Inset: corresponding logarithmic plot of current density versus voltage characteristics of electron-only devices.

Table 1
Photovoltaic parameters of PVSCs with different Cathode Configurations.

Cathode configuration	V_{oc} (V)	J_{sc} (mA/cm^2)	*FF* (%)	*PCE* (%)
PCBM/Ag	0.99 (0.97 ± 0.04)	17.56 (17.35 ± 0.45)	54.48 (51.20 ± 2.34)	9.51 (8.62 ± 0.43)
PCBM/F-R-COOK/Ag	1.08 (1.08 ± 0.02)	18.51 (17.89 ± 0.45)	72.13 (72.30 ± 1.85)	14.37 (13.94 ± 0.36)

tested. The photocurrent density-voltage (*J-V*) curves of the devices are shown in Fig. 3b and corresponding photovoltaic data of the devices are summarized in Table 1.

The devices without CBL gave a V_{oc} of 0.99 V, a J_{sc} of 17.56 mA/cm^2, an *FF* of 54.48%, and a maximum PCE of 9.51%. The *J-V* curve (Fig. 3a) exhibits an S-shape, which arises as a result of carrier accumulation inside the device [39]. The undesirable contact between the PCBM/Ag interface results in a relatively poor diode characteristics and a lower *FF* value. The insertion of F-R-COOK interlayers leads to a good rectification property as depicted by a higher V_{oc} of 1.08 V, an enhanced J_{sc} of 18.51% mA/cm^2, an increased *FF* of 72.13%, and a better PCE of 14.37%. In addition, low *J-V* hysteresis (Fig. 3b) upon forward and reverse device sweeping suggests that the perovskite active layer and interfaces have a negligible number of defects [40]. The enhancement in J_{sc} by inserting F-R-COOK layer consists well with EQE measurement. For the devices without CBL, the calculated J_{sc} is 17.59 mA/cm^2, which is in good agreement with the measured J_{sc} value of 17.56 mA/cm^2 in Fig. 3a. As shown in Fig. 3c, the EQE values in the entire photo response range between 300 nm and 750 nm are significantly enhanced after inserting the CBL, with peak values exceeding 70% between 380 nm and 730 nm. As a result, the calculated J_{sc} is determined to be 18.75 mA/cm^2, well in agreement with the measured J_{sc} value (18.51 mA/cm^2).

To get insight into the influence of electron injection efficiency at the PCBM/Ag interface, we fabricated electron-only devices with the following device configuration: ITO/ZnO/PCBM/F-R-COOK/Ag. As shown in Fig. 3d, the electron current density is significantly enhanced for F-R-COOK based devices when injected from the F-R-COOK/Ag electrode but is almost the same when injected from the ITO/ZnO electrode. This asymmetric change demonstrates that the increase in electron current density is attributed to the improved injection efficiency of the Ag electrode. Hence, F-R-COOK layer improved the electron injection current for Ag electrode compared to the devices with bare Ag electrode. We attribute this improvement to a reduced injection barrier at PCBM/Ag after inserting F-R-COOK layer.

Electrochemical impedance spectroscopy (EIS) technique is a powerful tool for analyzing the internal charge transfer behaviors in the perovskite solar cells. Fig. 4a shows the Nyquist plot of planar heterojunction perovskite solar cells. There is only one semicircle in the Nyquist plot, which means that the charge transfer and

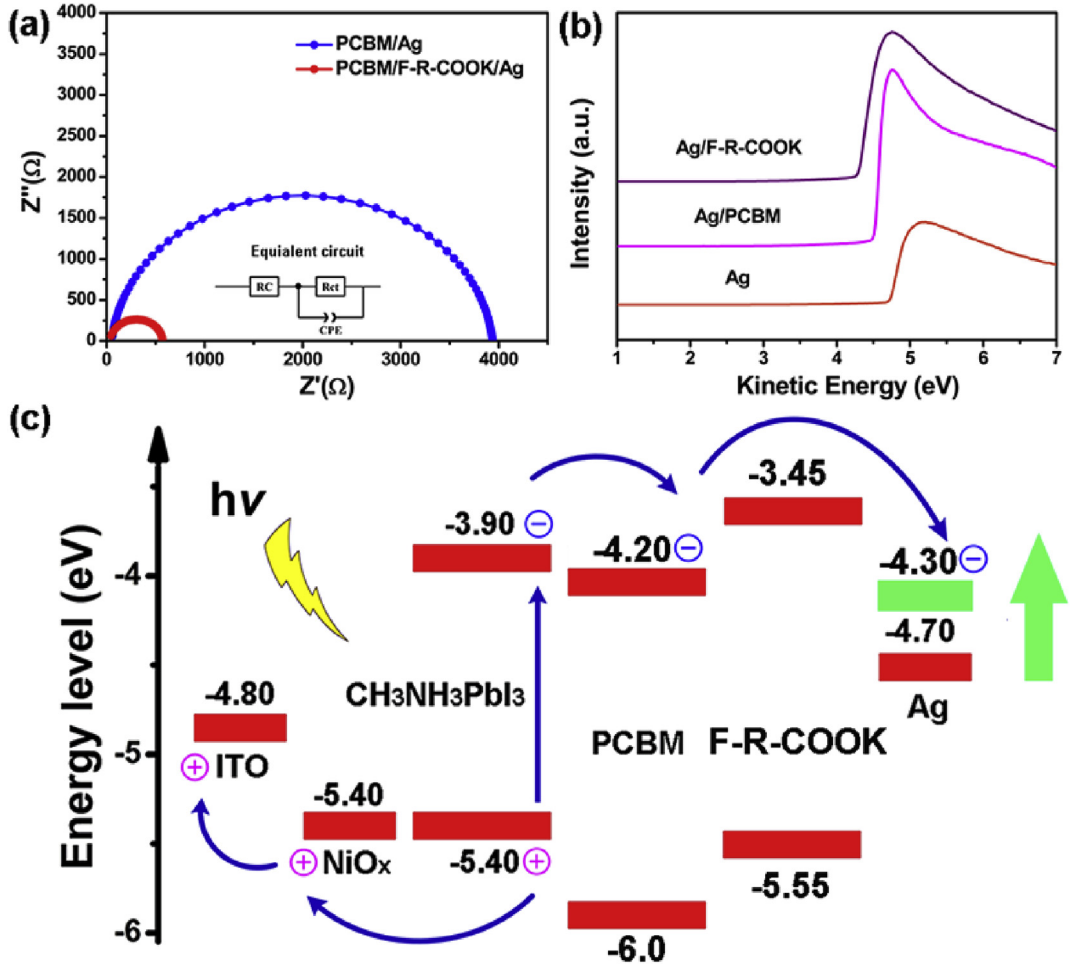

Fig. 4. (a)The Nyquist plot of planar heterojunction perovskite solar cells, (b)UPS spectra of Ag, Ag/PCBM and Ag/F-R-COOK thin films, c) Energy level diagram of the tested F-R-COOH and F-R-COOK.

accumulation processes in the devices can be simulated by a single RC unit. To improve the fittings, constant phase elements (CPE) are used instead of ideal capacitors. From the Nyquist plot fittings, the charge transfer resistance (Rct) for F-R-COOK/Ag device is 27 Ω cm^2, which is much smaller than that for the PCBM/Ag device (175 Ω cm^2). Smaller Rct for the F-R-COOK/Ag suggests that the electrons can more easily transport from PCBM layer to Ag cathode after inserting the F-R-COOK layer [37,41], since the device structure is almost the same for both the devices. This decrease in Rct and improvement in charge transport, after inserting the F-R-COOK layer, is well in agreement with the results obtained from electron only result.

In order to confirm a reduced injection barrier at PCBM/Ag by inserting F-R-COOK layer, we carried out ultraviolet photoelectron spectroscopy (UPS) measurements and determined the contact potential differences. Fig. 4b displays the results of UPS measurements for bare Ag, Ag/PCBM and Ag/F-R-COOK. The work function is 4.7 eV for bare Ag while it is 4.5 eV and 4.3 eV for Ag/PCBM and Ag/F-R-COOK, respectively. Obviously, the WF of the Ag electrode decreases from 4.7 to 4.3 eV when F-R-COOK interlayer is applied (Fig. 4c). The lower WF is attributed to the formation of large interfacial dipoles, by carboxylic potassium salt, which induce a vacuum-level shift modifying the WF of the Ag electrode [42,43]. Hence, lower WF of F-R-COOK/Ag cathode allows it to form ohmic contact with PCBM, which contributes to the higher V_{oc} value in the devices. Moreover, the lowered WF value of F-R-COOK/Ag could raise the built-in field, which increases the charge extraction efficiency and reduces the recombination losses [44].

An ESR spectroscopy was performed to further study the interface modification property. As shown in Fig. S4, no ESR signal was detected for F-R-COOK, revealing that no self-doping occur in F-R-COOK [45]. Meanwhile, blended samples of PCBM/F-R-COOK with the 1:1 weight ratio was tested to study the charge transfer property between the two components. In the PCBM/F-R-COOK blend, weak resonance peaks were detected. This result clearly suggests that electron transfer occurred from F-R-COOK to PCBM. The result from the ESR study provide the evidence that F-R-COOK could n-dope PCBM at the interface, leading to enhanced PVSCs device performance.

In addition to the PCE, the stability is another important aspect that needs to be improved for the practical application of PVSCs [46]. We investigated the stability of our devices in the ambient (Fig. S5). We found that the insertion of the F-R-COOK layer is helpful for enhancing the stability of the devices. As shown in Fig. S5, the PCE of the devices with CBL drop rapidly in the initial ≈100 h, ≈15% decrease on average. However, after storing for ≈100 h in air, the PCEs remained relatively stable even up to ≈200 h, still maintained 80% of the PCE. For the devices without CBL, a drastic decrease of the performance can be observed. Merely 33% of the PCE remained after ≈200 h of storage in air. These results indicate that the F-R-COOK CBL may have a blocking effect to water and/or oxygen to some extent, which is greatly helpful to improving the device stability.

4. Conclusion

In conclusion, we have successfully synthesized an alcohol soluble carboxylic potassium salt F-R-COOK and fabricated efficient p-i-n PHJ PVSCs using F-R-COOK as CBL material. A variety of electrical and surface potential characterization techniques were used to understand the interfacial effects between the metal electrode and CBL. Its higher charge transport efficiency and work function tuning effect help to improve the performance of the perovskite solar cells. A PCE of 14.37% is obtained for the F-R-COOK-based devices, which is much higher than that of the Ag-only device (9.51%). Our results demonstrate that F-R-COOK might be a potential candidate as electrode modification layer in solution-processed inverted perovskite solar cells.

Notes

The authors declare no competing financial interest.

Acknowledgements

The authors are thankful to Dr. Imran Murtaza for assistance in preparing the manuscript. This work was financially supported by Shenzhen Science and Technology Research Grant (JCYJ20160510144254604, JCYJ20150331100628880), the Shenzhen Peacock Plan (KQTD20140627145432 96), Guangdong Key Research Project (Nos. 2014B090914003, 2015B090914002), National Basic Research Program of China (973 Program, No. 2015CB856505), Natural Science Foundation of Guangdong Province (2014A030313800) and Guangdong Academician Workstation (2013B090400016).

Appendix A. Supplementary data

Supplementary data related to this article can be found at http://dx.doi.org/10.1016/j.orgel.2017.02.041.

References

[1] F. Huang, H. Wu, Y. Cao, Water/alcohol soluble conjugated polymers as highly efficient electron transporting/injection layer in optoelectronic devices, Chem. Soc. Rev. 39 (2010) 2500–2521.
[2] J. Mei, Y. Diao, A.L. Appleton, L. Fang, Z. Bao, Integrated materials design of organic semiconductors for field-effect transistors, J. Am. Chem. Soc. 135 (2013) 6724–6746.
[3] Z. He, H. Wu, Y. Cao, Recent advances in polymer solar cells: realization of high device performance by incorporating water/alcohol-soluble conjugated polymers as electrode buffer layer, Adv. Mater. 26 (2014) 1006–1024.
[4] H. Kim, K.-G. Lim, T.-W. Lee, Planar heterojunction organometal halide perovskite solar cells: roles of interfacial layers, Energy Environ. Sci. (2016) 12–30.
[5] Z. Zhou, S. Pang, Z. Liu, H. Xu, G. Cui, Interface engineering for high-performance perovskite hybrid solar cells, J. Mater. Chem. A 3 (2015) 19205–19217.
[6] W. Wang, M.O. Tade, Z. Shao, Research progress of perovskite materials in photocatalysis- and photovoltaics-related energy conversion and environmental treatment, Chem. Soc. Rev. 44 (2015) 5371–5408.
[7] N.H. Tiep, Z. Ku, H.J. Fan, Recent advances in improving the stability of perovskite solar cells, Adv. Energy Mater. 44 (2015) 5371–5408.
[8] S. Shi, Y. Li, X. Li, H. Wang, Advancements in all-solid-state hybrid solar cells based on organometal halide perovskites, Mater. Horiz. 2 (2015) 378–405.
[9] L. Meng, J. You, Y. Yang, J. You, T.-F. Guo, Recent advances in the inverted planar structure of perovskite solar cells, Acc. Chem. Res. 49 (2016) 155–165.
[10] C.-C. Chueh, C.-Z. Li, A.K.Y. Jen, Recent progress and perspective in solution-processed Interfacial materials for efficient and stable polymer and organometal perovskite solar cells, Energy Environ. Sci. 8 (2015) 1160–1189.
[11] T.C. Sum, N. Mathews, Advancements in perovskite solar cells: photophysics behind the photovoltaics, Energy Environ. Sci. 7 (2014) 2518–2534.
[12] M.A. Green, A. Ho-Baillie, H.J. Snaith, The emergence of perovskite solar cells, Nat. Photonics 8 (2014) 506–514.
[13] S. Kazim, M.K. Nazeeruddin, M. Graetzel, S. Ahmad, Perovskite as light harvester: a game changer in photovoltaics, Angew. Chem. Int. Ed. 53 (2014) 2812–2824.
[14] G. Xing, N. Mathews, S. Sun, S.S. Lim, Y.M. Lam, M. Grätzel, S. Mhaisalkar, T.C. Sum, Long-range balanced electron- and hole-transport lengths in organic-inorganic CH3NH3PbI3, Science 342 (2013) 344–347.
[15] S.D. Stranks, G.E. Eperon, G. Grancini, C. Menelaou, M.J.P. Alcocer, T. Leijtens, L.M. Herz, A. Petrozza, H.J. Snaith, Electron-hole diffusion lengths exceeding 1 micrometer in an organometal trihalide perovskite absorber, Science 342 (2013) 341–344.
[16] A. Kojima, K. Teshima, Y. Shirai, T. Miyasaka, Organometal halide perovskites as visible-light sensitizers for photovoltaic cells, J. Am. Chem. Soc. 131 (2009) 6050–6051.
[17] P. Docampo, J.M. Ball, M. Darwich, G.E. Eperon, H.J. Snaith, Efficient organometal trihalide perovskite planar-heterojunction solar cells on flexible polymer substrates, Nat. Commun. 4 (2013) 2761.
[18] Research Cell Efficiency Records, NREL, http://www.nrel.gov/ncpv/. (Accessed on August 2016).

[19] N.J. Jeon, H.G. Lee, Y.C. Kim, J. Seo, J.H. Noh, J. Lee, S.I. Seok, o-Methoxy substituents in spiro-OMeTAD for efficient inorganic–organic hybrid perovskite solar cells, J. Am. Chem. Soc. 136 (2014) 7837–7840.
[20] S. Ryu, J.H. Noh, N.J. Jeon, Y. Chan Kim, W.S. Yang, J. Seo, S.I. Seok, Voltage output of efficient perovskite solar cells with high open-circuit voltage and fill factor, Energy Environ. Sci. 7 (2014) 2614–2618.
[21] Z. Xiao, C. Bi, Y. Shao, Q. Dong, Q. Wang, Y. Yuan, C. Wang, Y. Gao, J. Huang, Efficient, high yield perovskite photovoltaic devices grown by interdiffusion of solution-processed precursor stacking layers, Energy Environ. Sci. 7 (2014) 2619–2623.
[22] Q. Wang, Y. Shao, Q. Dong, Z. Xiao, Y. Yuan, J. Huang, Large fill-factor bilayer iodine perovskite solar cells fabricated by a low-temperature solution-process, Energy Environ. Sci. 7 (2014) 2359–2365.
[23] J.-Y. Jeng, Y.-F. Chiang, M.-H. Lee, S.-R. Peng, T.-F. Guo, P. Chen, T.-C. Wen, CH3NH3PbI3 perovskite/fullerene planar-heterojunction hybrid solar cells, Adv. Mater. 25 (2013) 3727–3732.
[24] J. You, Z. Hong, Y. Yang, Q. Chen, M. Cai, T.-B. Song, C.-C. Chen, S. Lu, Y. Liu, H. Zhou, Y. Yang, Low-temperature solution-processed perovskite solar cells with high efficiency and flexibility, ACS Nano 8 (2014) 1674–1680.
[25] J.H. Seo, A. Gutacker, Y. Sun, H. Wu, F. Huang, Y. Cao, U. Scherf, A.J. Heeger, G.C. Bazan, Improved high-efficiency organic solar cells via incorporation of a conjugated polyelectrolyte interlayer, J. Am. Chem. Soc. 133 (2011) 8416–8419.
[26] T.M. Khan, Y. Zhou, A. Dindar, J.W. Shim, C. Fuentes-Hernandez, B. Kippelen, Organic photovoltaic cells with stable top metal electrodes modified with polyethylenimine, ACS Appl. Mat. Interfaces 6 (2014) 6202–6207.
[27] J. Seo, S. Park, Y. Chan Kim, N.J. Jeon, J.H. Noh, S.C. Yoon, S.I. Seok, Benefits of very thin PCBM and LiF layers for solution-processed p-i-n perovskite solar cells, Energy Environ. Sci. 7 (2014) 2642–2646.
[28] Y. Deng, E. Peng, Y. Shao, Z. Xiao, Q. Dong, J. Huang, Scalable fabrication of efficient organolead trihalide perovskite solar cells with doctor-bladed active layers, Energy Environ. Sci. 8 (2015) 1544–1550.
[29] H. Zhang, H. Azimi, Y. Hou, T. Ameri, T. Przybilla, E. Spiecker, M. Kraft, U. Scherf, C.J. Brabec, Improved high-efficiency perovskite planar heterojunction solar cells via incorporation of a polyelectrolyte interlayer, Chem. Mater. 26 (2014) 5190–5193.
[30] P.-W. Liang, C.-Y. Liao, C.-C. Chueh, F. Zuo, S.T. Williams, X.-K. Xin, J. Lin, A.K.Y. Jen, Additive enhanced crystallization of solution-processed perovskite for highly efficient planar-heterojunction solar cells, Adv. Mater. 26 (2014) 3748–3754.
[31] C.-Y. Chang, Y.-C. Chang, W.-K. Huang, K.-T. Lee, A.-C. Cho, C.-C. Hsu, Enhanced performance and stability of semitransparent perovskite solar cells using solution-processed thiol-functionalized cationic surfactant as cathode buffer layer, Chem. Mater. 27 (2015) 7119–7127.
[32] C.-Y. Chang, W.-K. Huang, J.-L. Wu, Y.-C. Chang, K.-T. Lee, C.-T. Chen, Room-temperature solution-processed n-doped zirconium oxide cathode buffer layer for efficient and stable organic and hybrid perovskite solar cells, Chem. Mater. 28 (2016) 242–251.
[33] Q. Xue, Z. Hu, J. Liu, J. Lin, C. Sun, Z. Chen, C. Duan, J. Wang, C. Liao, W.M. Lau, F. Huang, H.-L. Yip, Y. Cao, Highly efficient fullerene/perovskite planar heterojunction solar cells via cathode modification with an amino-functionalized polymer interlayer, J. Mater. Chem. A 2 (2014) 19598–19603.
[34] Y. Liu, M. Bag, L.A. Renna, Z.A. Page, P. Kim, T. Emrick, D. Venkataraman, T.P. Russell, Understanding interface engineering for high-performance fullerene/perovskite planar heterojunction solar cells, Adv. Energy Mater. 6 (2016) 1501606.
[35] J. Min, Z.-G. Zhang, Y. Hou, C.O. Ramirez Quiroz, T. Przybilla, C. Bronnbauer, F. Guo, K. Forberich, H. Azimi, T. Ameri, E. Spiecker, Y. Li, C.J. Brabec, Interface engineering of perovskite hybrid solar cells with solution-processed perylene-diimide heterojunctions toward high performance, Chem. Mater. 27 (2015) 227–234.
[36] K.-G. Lim, H.-B. Kim, J. Jeong, H. Kim, J.Y. Kim, T.-W. Lee, Boosting the power conversion efficiency of perovskite solar cells using self-organized polymeric hole extraction layers with high work function, Adv. Mater. 26 (2014) 6461–6466.
[37] K. Wang, C. Liu, C. Yi, L. Chen, J. Zhu, R.A. Weiss, X. Gong, Efficient perovskite hybrid solar cells via ionomer interfacial engineering, Adv. Funct. Mater. 25 (2015) 6875–6884.
[38] J. You, L. Meng, T.-B. Song, T.-F. Guo, Y. Yang, W.-H. Chang, Z. Hong, H. Chen, H. Zhou, Q. Chen, Y. Liu, N. De Marco, Y. Yang, Improved air stability of perovskite solar cells via solution-processed metal oxide transport layers, Nat. Nano 11 (2016) 75–81.
[39] B. Qi, J. Wang, Fill factor in organic solar cells, PCCP 15 (2013) 8972–8982.
[40] H.J. Snaith, A. Abate, J.M. Ball, G.E. Eperon, T. Leijtens, N.K. Noel, S.D. Stranks, J.T.-W. Wang, K. Wojciechowski, W. Zhang, Anomalous hysteresis in perovskite solar cells, J. Phy. Chem. Lett. 5 (2014) 1511–1515.
[41] Y. Bai, H. Chen, S. Xiao, Q. Xue, T. Zhang, Z. Zhu, Q. Li, C. Hu, Y. Yang, Z. Hu, F. Huang, K.S. Wong, H.-L. Yip, S. Yang, Effects of a molecular monolayer modification of NiO nanocrystal layer surfaces on perovskite crystallization and interface contact toward faster hole extraction and higher photovoltaic performance, Adv. Funct. Mater. 26 (2016) 2950–2958.
[42] Q. Zhang, D. Zhang, X. Li, X. Liu, W. Zhang, L. Han, J. Fang, Neutral amine based alcohol-soluble interface materials for inverted polymer solar cells: realizing high performance and overcoming solvent erosion, Chem. Commun. 51 (2015) 10182–10185.
[43] H.-L. Yip, A.K.Y. Jen, Recent advances in solution-processed interfacial materials for efficient and stable polymer solar cells, Energy Environ. Sci. 5 (2012) 5994–6011.
[44] Z.-G. Zhang, B. Qi, Z. Jin, D. Chi, Z. Qi, Y. Li, J. Wang, Perylene diimides: a thickness-insensitive cathode interlayer for high performance polymer solar cells, Energy Environ. Sci. 7 (2014) 1966–1973.
[45] Z. Wu, C. Sun, S. Dong, X.-F. Jiang, S. Wu, H. Wu, H.-L. Yip, F. Huang, Y. Cao, n-Type water/alcohol-soluble naphthalene diimide-based conjugated polymers for high-performance polymer solar cells, J. Am. Chem. Soc. 138 (2016) 2004–2013.
[46] C. Qin, T. Matsushima, T. Fujihara, W.J. Potscavage, C. Adachi, Degradation mechanisms of solution-processed planar perovskite solar cells: thermally stimulated current measurement for analysis of carrier traps, Adv. Mater. 28 (2016) 466–471.